24th November 1997 CB-Note 317

Technical Report

Study of $\bar{p}p$-annihilations at rest in liquid and gaseous hydrogen into $\pi^0\pi^0\eta$ with evidence for an exotic isovector 1^{-+}-wave

Mario Herz

ISKP/University Bonn

Nussallee 14-16

D-53115 Bonn

1 Introduction

The $\pi^0\pi^0\eta$ final state of protonium annihilation at rest where antiprotons of incident beam momentum of 210 MeV/c are stopped in liquid or gaseous hydrogen provides a platform for the investigation of the existence of $\eta\pi$-waves carrying exotic quantum numbers such as $I^G(J^{PC})=1^-(1^{-+})$.

Data on this particular final state have been collected from annihilations into six photons detected with the Crystal Barrel detector at LEAR/CERN. Figure 2 shows the Dalitz plots of this 3-body-final state for both target types. The high statistics data sample from annihilations in liquid hydrogen cover 306 491 events from 15 174 690 all-neutral events. 13 239 623 all-neutral events from annnihilations in gaseous hydrogen of the nov'94 run period led to 269 087 $\pi^0\pi^0\eta$-events.

The prominent features of the data are due to the $a_0(980)$, $a_0(1450)$, $a_2(1320)$, $a_2(1650)$ and $f_0(980)$ of the underlying scalar $(\pi\pi)$-interactions. Further contributions of a $(\eta\pi)_P$-wave revealing evidence of an exotic state called $\hat{\rho}(1390)$ are subject of the investigations reported here. The evidence for the exotic state, finally, originates from missing intensity when describing data and from the interference pattern with the two well known resonances $a_2(1320)$ and $f_0(980)$. The contributions from each allowed $\bar{p}p$-initial state with angular momentum lower than L=2 are constrained by cascade model calculations [3] and by the results of a discussion of branching ratios [4]. The ratios of the annihilation rate per initial state when switching from liquid to gaseous hydrogen is given in table 1. It turns out that 90% of all annihilations in liquid hydrogen occure from initial $^1S_0$-state, the other two allowed initial $^3P_1$- and $^3P_2$-states contribute almost equally to the final state delivering the remaining intensity. In gaseous hydrogen the $^1S_0$-state covers 60% of all intensity versus 40% for the ^3P-states.

The partial wave analysis assigns 1-4% of all intensity to the state carrying the exotic quantum numbers $I^G(J^{PC})=1^-(1^{-+})$ which are forbidden for common quarkonia. There is further intensity from interferences with the above named resonances in the order of 10%. Mass and width of this state from a Breit-Wigner-parametrization are $M=(1385 \pm 15)$ MeV/c^2 and $\Gamma=150^{+100}_{-50}$ MeV/c^2.

2 Data selection

In the run period november '94 a high pressure gas target was used in the center of the Crystal Barrel detector to measure protonium annihilations at 12 atm. The aim of this measurement was to obtain data sets of all-neutral final states compatible in statistics to those derived from annihilations in liquid hydrogen. This way the fraction of annihilations from atomic P-state can be determined in dependence of the target pressure.

2.1 Preselection

All-neutral-triggered data events with any remaining track due to trigger inefficiencies get rejected in the first step of data preselection. To identify π^0 and η we use their $\gamma\gamma$-decay mode. Hence, we require six unmatched PEDs in the electromagnetic calorimeter. The algorithm TAXI identifies events containing hadronic split-offs, DOLBY-C scans for electromagnetic split-offs where corresponding PEDs are dropped. The GOLDEN γ definition is applied with the thresholds for the energy of the central crystal (CC), the PED energy and the cluster energy set to E(CC) > 13 MeV, E(PED) > 13 MeV, E(cluster) > 14 MeV and the ratio $E_1/E_9 < 0.96$. Crystal type #13 events are rejected as well. After all cuts we are left with 9 679 936 accepted events which are submitted to the kinematic fit.

2.2 Kinematic fit

The $\pi^0\pi^0\eta$ final state is detected in its 6γ mode with each meson decaying into 2γ. The flat confidence level distribution of the 4C-fit requiring energy- and momentum conservation is shown in figure 1a. Figures 1b, 1c and 1d show the PULLs for total energy, the azimuthal angle Φ and the polar angle Θ respectively. The latter ones represent a normal distribution with $\sigma = 1$ whereas the distribution for the energy is asymmetric as expected due to loss of energy of electromagnetic showers. In order to select the $\pi^0\pi^0\eta$ final state from the other main 6γ-final states, $\pi^0\pi^0\pi^0$ and $\pi^0\eta\eta$, we require the confidence level for

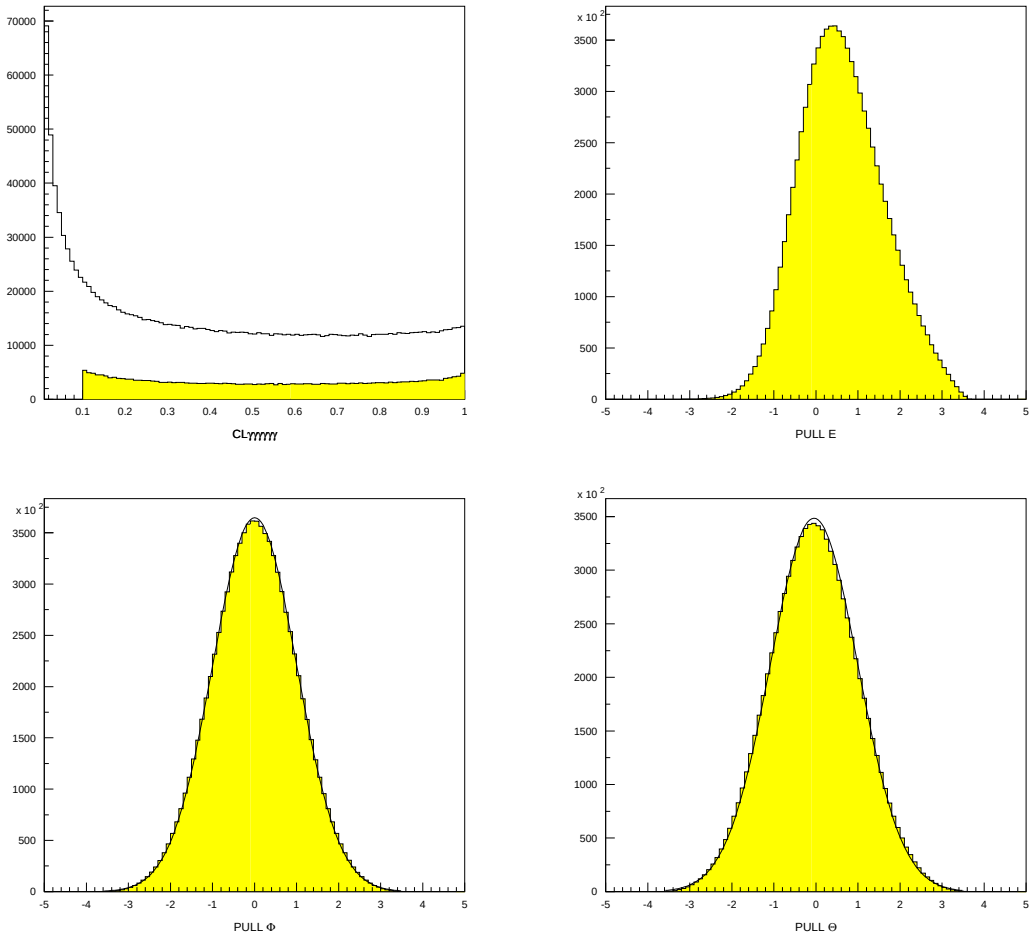

Figure 1: *Confidence Level (a, upper left), $PULL_E$ (b, upper right), $PULL_\Phi$ (c, bottom left) und $PULL_\Theta$ (d, bottom right) of the kinematic fit with 6γ-hypothesis*

this hypothesis (7C) to be larger than 10% and larger than every one of the others. Its distribution is shown in the inset of figure 1a.

2.3 The $\pi^0\pi^0\eta$ final state

For comparison reasons the two Dalitz plots of the $\pi^0\pi^0\eta$ final state from annihilations in liquid and in gaseous hydrogen are shown in figure 2. The most prominent structures in our data are due to $a_0(980)$, $a_2(1320)$ and $f_0(980)$ besides the isoscalar scalar $(\pi\pi)$-wave. Further two resonances, $a_0(1450)$ and $a_2(1650)$, are known already from previous analyses. Evidence for an exotic wave in the $(\eta\pi)$-system will be discussed in this note.

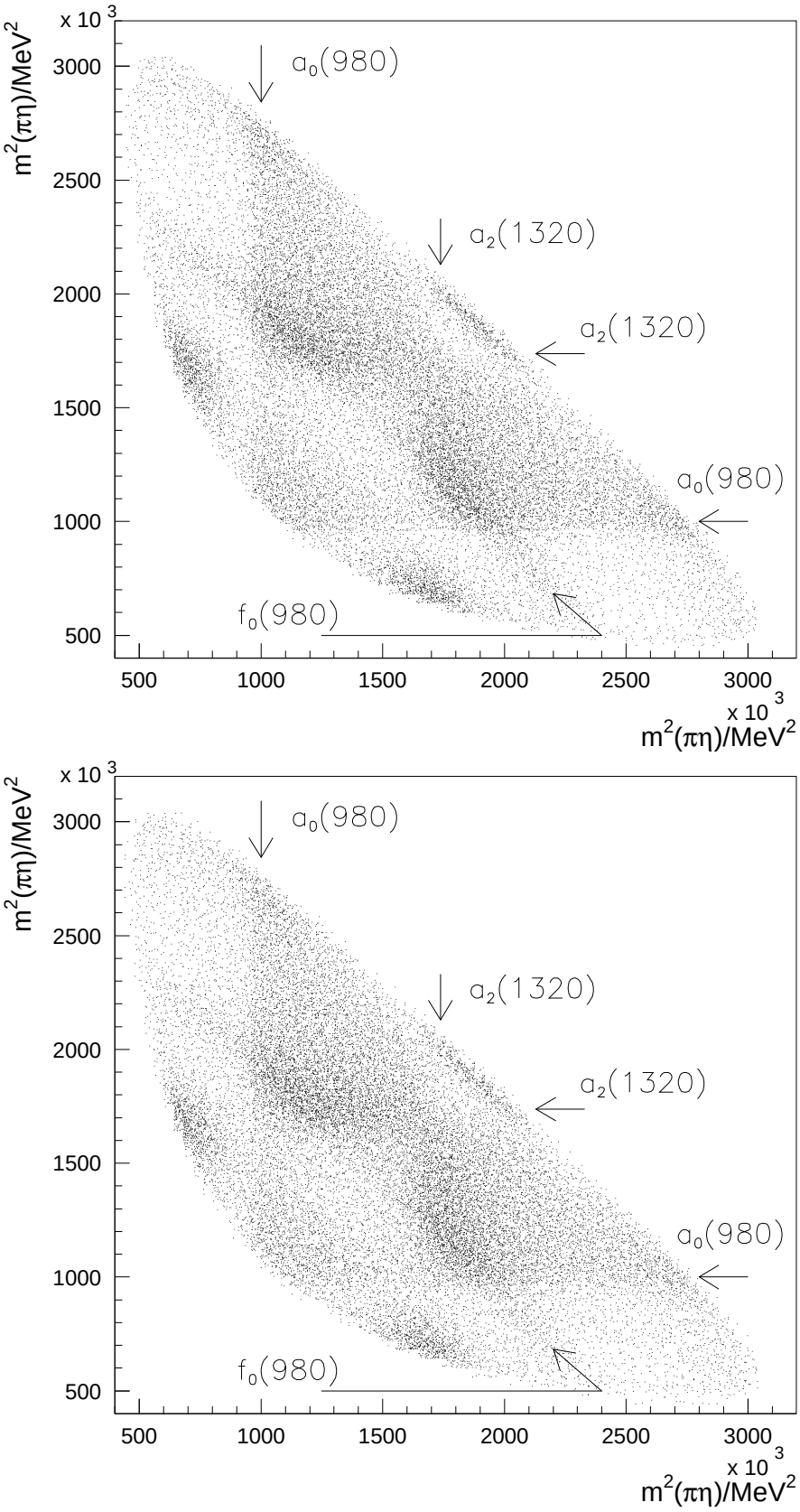

Figure 2: Dalitz plots of $\bar{p}p$ annihilations at rest into $\pi^0\pi^0\eta$ for antiprotons stopping in liquid hydrogen (upper) and gaseous hydrogen at 12 atm (lower)

3 Monte-Carlo studies

From previous work the acceptance Dalitz plot for liquid hydrogen data was available. In order to simulate the phase space distribution for the reaction $\bar{p}p \rightarrow \pi^0\pi^0\eta$ from annihilations in gaseous hydrogen we generated 438 113 (N_{MC}) Monte-Carlo-Events using the $\bar{p}$-stop distribution measured in gas. All events were fed through the same selection chains as described for real data. We were left with 282 000 events in the acceptance Dalitz plot ($N_{\pi^0\pi^0\eta-mc}$). Figure 3 shows the acceptance correction Dalitz plots for liquid and gaseous hydrogen data. They both are flat except at the kinematical boundaries where fluctuations of 2-4% occur.

The evaluation of the reconstruction efficiency in gaseous hydrogen leads to $\epsilon_L=(26.7 \pm 1.4)\%$ and $\epsilon_G=(28.7 \pm 1.7)\%$. There is a statistical uncertainty of less than 0.1% due to missinterpreted $\pi^0\pi^0\pi^0$- or $\pi^0\eta\eta$-events. The decay probability for the 2γ-decays of π^0 and η are 0.988 and 0.3925, respectively, for which the number of reconstructed events $N_{\pi^0\pi^0\eta}$ has to be corrected. The branching ratio for the reaction $\bar{p}p \rightarrow \pi^0\pi^0\eta$ can be derived in the following way

$$BR(\bar{p}p \rightarrow \pi^0\pi^0\eta) = \frac{N_{\pi^0\pi^0\eta}}{N_{AN-trig}} \times \frac{N_{AN}}{N_{MB}} \times \frac{1}{\epsilon} \tag{1}$$

where the number of all neutral events in minimum bias data, N_{AN}/N_{MB}, was determined in comparing the number of $\pi^0\pi^0$-events in all-neutral triggered data versus the number of $\pi^0\pi^0$-events in minimum bias triggered data. For annihilations in liquid hydrogen one finds a fraction of $N_{AN}/N_{MB}=(3.14 \pm 0.25)\%$. For annihilations in gaseous hydrogen the fraction was determined to $N_{AN}/N_{MB}=(3.32 \pm 0.28)\%$ [8]. There are 306 491 events left when selecting the $\pi^0\pi^0\eta$ final state from 15 174 690 all-neutral events taken in liquid hydrogen. In gaseous hydrogen we find 269 087 events from 13 239 623 triggered events. The branching ratios therefore read

$$BR(\bar{p}p \rightarrow \pi^0\pi^0\eta)_{LH2} = (6.20 \pm 0.68) \times 10^{-3} \tag{2}$$

$$BR(\bar{p}p \rightarrow \pi^0\pi^0\eta)_{GH2} = (6.14 \pm 0.67) \times 10^{-3} \tag{3}$$

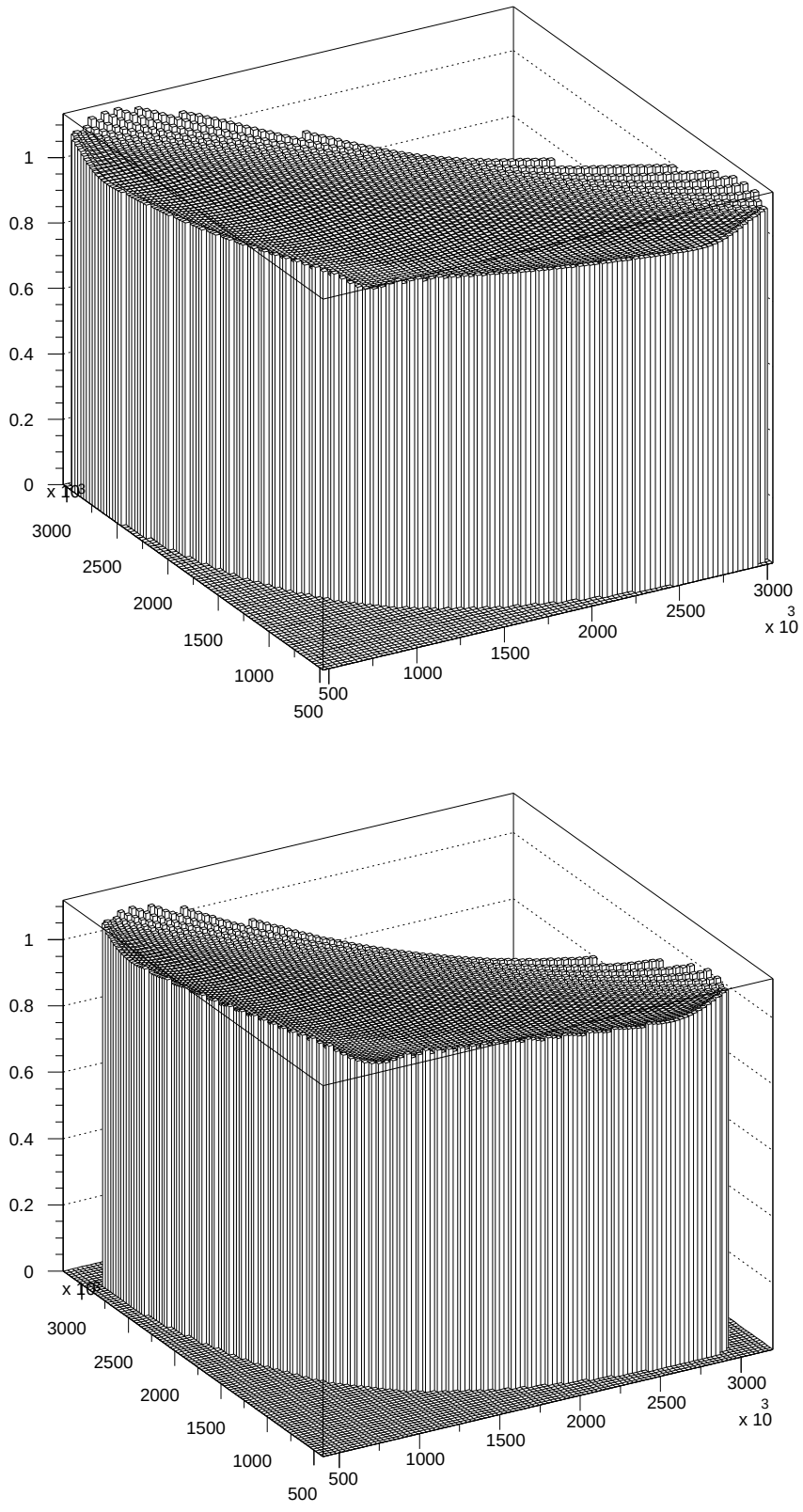

Figure 3: Monte Carlo Acceptance Dalitz plots of $\bar{p}p$ annihilations at rest into $\pi^0\pi^0\eta$ for antiprotons stopping in liquid hydrogen (upper) and gaseous hydrogen at 12 atm (lower)

4 Protonium

Antiprotons from LEAR hit the hydrogen target of our detector and loose energy due to electromagnetic interaction. As soon as the $\bar{p}$-energy has suitably dropped down to few eV the antiproton can get captured in a hydrogen molecule emitting one of its electrons [1]. When falling apart a Rhydberg like atomic protonium state with principle quantum numbers $n \approx 30$ is left. Such highly excited states loose energy by chemical effects, external Auger effect or radiative transitions. The relative distance between proton and antiproton drops down rapidly due to increased reduced mass compared to a hydrogen atom. Such protonium states are much smaller than ordinary hydrogen atoms and therefore are exposed strong electric fields when passing through neighboring hydrogen molecules. This leads to mixing of angular momentum states for given principle quantum number due to Stark effect.

In liquid hydrogen where target density is large Stark effect dominates. Thus, rapid transfer to atomic S- and P-states occurs even for large quantum numbers n. Annihilations from S-states dominate compared to annihilations from P-states. Contributions from atomic D-waves are negligible for annihilations at rest.

The more the target density is decreased the more the time gets enlarged the protonium bound state needs to reach the ever next hydrogen molecule providing a strong electric field. Thus, Stark mixing gets reduced and the probability of S-state annihilations drops down. In parallel annihilations from P-states contribute more to the final states.

In the case of very small pressures (vaccum) the protonium system cascades down due to radiative transitions preferentially along the states of angular momentum l=n-1. Such a circular cascade stopps by protonium annihilation from 2P-state in 99% of all cases.

There are six atomic levels below D-wave

$$^1S_0 \quad ^3S_1 \quad ^1P_1 \quad ^3P_0 \quad ^3P_1 \quad ^3P_2 \tag{4}$$

carrying the quantum numbers

$$0^{-+} \quad 1^{--} \quad 1^{+-} \quad 0^{++} \quad 1^{++} \quad 2^{++}. \tag{5}$$

S-states are calculated to have widths in the order of KeV whereas P-states have widths in the order of meV with $^3P_0$ being broader by a factor of about 5 in comparison to the other

^3P_J-states due to tensor forces [2]. For high target pressures with dominating Stark effect high annihilation rates from high-n S-states with maximum overlap of the wave functions for proton and antiproton can be expected because mixing of angular momentum states assures rapid repopulation of low-l states after annihilation. In low pressure targets with decreased Stark effect antiprotons cascade down to lower n-states ($n \geq 2$). According to [3] one obtains from atomic physics based cascade model calculations the fractions of annihilation rates for each initial protonium state when switching from liquid hydrogen to gaseous hydrogen targets (15 atm) as given in the upper line of table 1. [4] reports on two-body branching ratios as probes for definite initial states and measured for varying target pressures. This gives in an analogue way the fractions of annihilation rates plus errors from measurement.

$^{2S+1}L_J$	$^1S_0$	$^3S_1$	$^1P_1$	$^3P_0$	$^3P_1$	$^3P_2$
F	0.64	0.66	3.73	1.81	4.27	3.46
F	0.67 ± 0.1	0.64 ± 0.12	3.0 ± 1.5	2.1 ± 0.6	$2.0^{+3.0}_{-1.4}$	5.0 ± 3.0

Table 1: *annihilation rates of each protonium initial state*

This set of numbers have been used as scaling parameters of the production strengths when analysing both data sets of protonium annihilations into the final state $\pi^0\pi^0\eta$.

5 Partial wave analysis

The 3-body final state $\pi^0\pi^0\eta$ will be described according to the Isobar Model. In a first step a $(\pi^0\pi^0)$- or a $(\pi^0\eta)$- resonance with quantum numbers l^{pc} is produced recoiling against an η or π^0 meson, respectively. The $(\pi^0\pi^0)$-resonance may have quantum numbers 0^{++} or 2^{++} for angular momentum l=1 between two π^0 is forbidden by Bose-Symmetry. The angular momentum between π^0 and η may be l=0, l=1 or l=2 corresponding to l^{pc} quantum numbers 0^{++}, 1^{-+} or 2^{++}, respectively. Note that quantum numbers 1^{-+} are forbidden for $\mathrm{q\bar{q}}$-mesons.

The resonances decay into two pseudoscalar mesons. We have chosen the K-matrix formalism to describe production and decays of resonances which guarantees conservation of unitarity and of time reversal invariance for symmetric and real K-matrices. The K-matrix is related to the more familiar scattering amplitude T via

$$T = (I - 2\imath K)^{-1} K \tag{6}$$

in case of elastic scattering, the T-matrix is of modulus one but not relativistically invariant. It is therefore more appropiate to use the invariant form $\hat{T}$. It differs from its noninvariant form by the inclusion of phase space factors

$$T_{ij} = \{\rho_i\} \hat{T_{ij}} \{\rho_j\}. \tag{7}$$

In $\bar{\mathrm{p}}\mathrm{p}$-annihilations at rest resonances are not formed due to scattering; resonances are *produced*. Therefore we assign production strengths to each individual resonance which are described by a production vector $\hat{P}$. This way one obtains the production amplitude

$$\hat{F^l} = (I - \imath \hat{K})^{-1} \hat{P}. \tag{8}$$

The overall transition amplitude for protonium annihilation at rest then reads

$$\mathcal{A} = \sum Z_{J^{PC},L,l} \cdot \hat{F^l} \cdot B^L \tag{9}$$

where Z stands for the coupled angular distribution of the overall process. The dynamical part is represented by the function F^l times a centrifugal barrier factor B^L for the isobar production. More details can be found in [5].

Both data sets are fitted simultaneously. For each one of the allowed initial protonium states $^1S_0$, $^3P_1$ and $^3P_2$, there is a unique decay amplitude for annihilations in liquid and gaseous hydrogen. In the analysis presented here we reduce the number of free parameters in fixing the ratios of these amplitudes for both data sets according to the values given in table 1. The ratios were derived from comparisons of branching ratios of 2-body-final states as probes for definite initial states. A full description of data is ensured when introducing

- 2 scalar isovector resonances, $a_0(980)$ and $a_0(1450)$
- 2 tensor isovector resonances, $a_2(1320)$ and $a_2(1650)$
- 1 scalar isoscalar wave of $(\pi\pi)$-interactions including $f_0(980)$and $f_0(1370)$
- 1 tensor isoscalar resonance, $f_2(1270)$
- 1 vector isovector resonance, $\hat{\rho}$

The $(\pi\pi)_S$-wave is derived from a reanalysis of the $\pi^0\pi^0\pi^0$ data from liquid hydrogen. The amplitude is constrained by $(\pi\pi)_S$-wave scattering data from earlier experiments [6]. It is kept fixed except in a last step of the fit when the $(\pi\pi)_S$-wave parametrization is left free in order to find the best fit. This changes the $f_0(980)$ parameters slightly. The limited $(\pi\pi)$-phase space in this data does not provide much information on the higher-mass part of the $(\pi\pi)$-scattering amplitude, hence we keep mass and width of the $f_0(1370)$ in accordance to the data of the scattering phase. Presence of $a_0(980)$ and $a_2(1320)$ is obvious. Evidence for $a_0(1450)$ is statistically significant due to decrease in χ^2 by 3423 units (2810 units for LH_2-data and 613 units for GH_2-data). Introduction of $a_2(1650)$ is demanded in the fit by 3050 units (1050 units for LH_2-data and 2000 units for GH_2-data). There is weak evidence for the $f_2(1270)$ with mass and width fixed to nominal values [7] leading to a χ^2 difference of 458 units (152 units in LH_2-data and 306 units in GH_2-data). The evidence for the exotic state wave will be discussed later on in more detail.

The above maximal set of resonances satisfies the requirements of a good fit to data as shown in figure 4 and figure 5 with $\chi^2/N_{dof} = 5037/3475$ for liquid hydrogen data and in figure 6 and figure 7 with $\chi^2/N_{dof} = 2386/1744$ for gaseous hydrogen data. Therefore one is left with checking systematically the production mechanism.

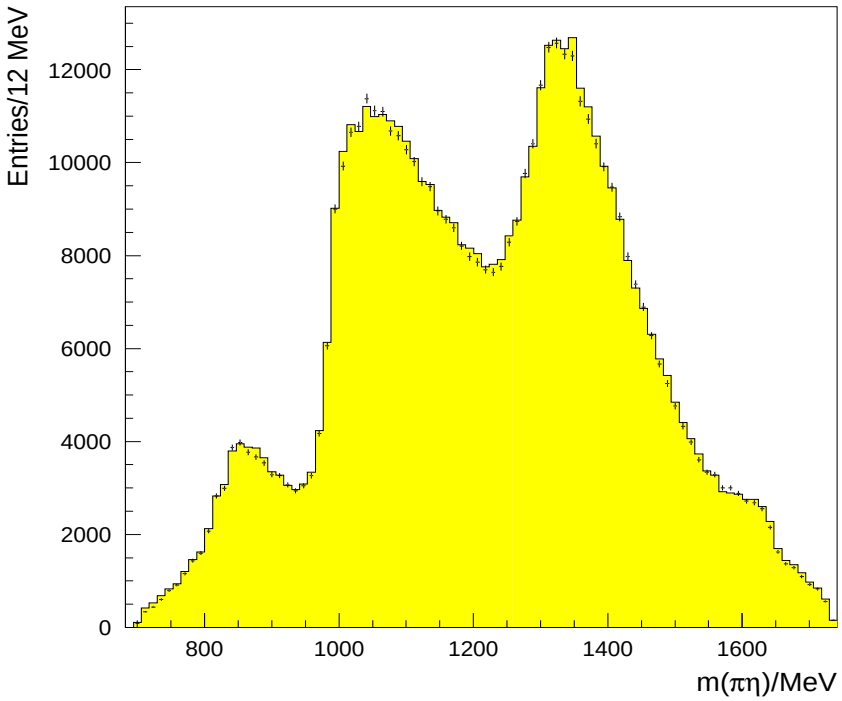

Figure 4: *Fit* $\bar{p}p \to \pi^0\pi^0\eta$ *in projection onto* $(\eta\pi)$*-system for liquid hydrogen data*

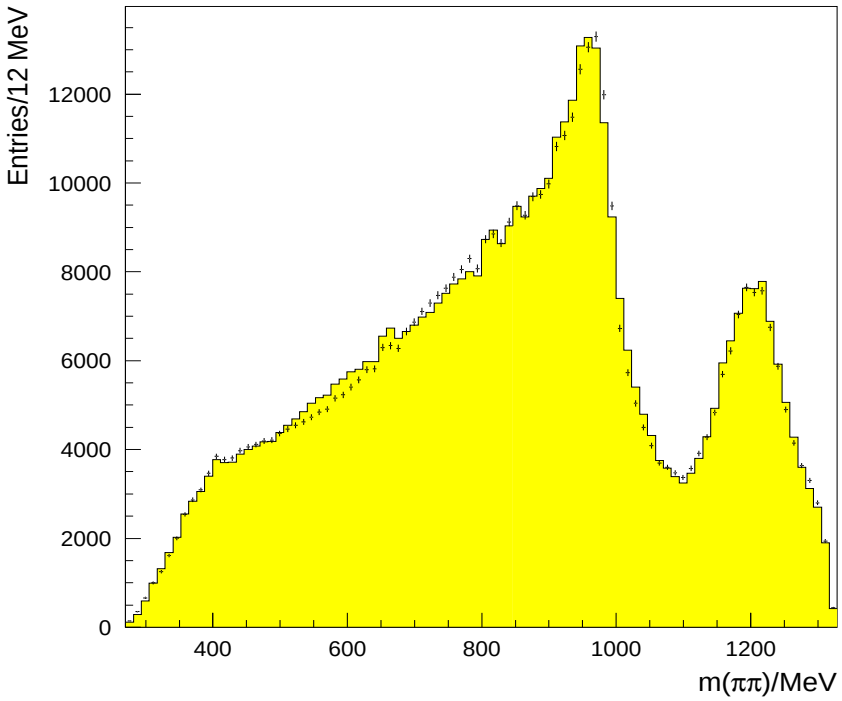

Figure 5: *Fit* $\bar{p}p \to \pi^0\pi^0\eta$ *in projection onto* $(\pi\pi)$*-system for liquid hydrogen data*

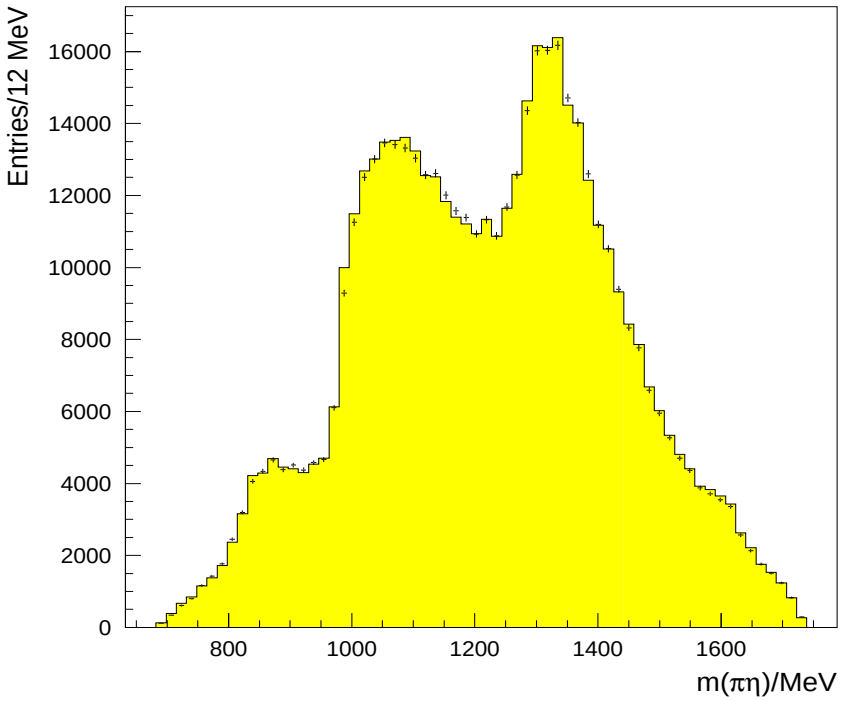

Figure 6: *Fit $\bar{p}p \to \pi^0\pi^0\eta$ in projection onto the $(\eta\pi)$-system for gaseous hydrogen data*

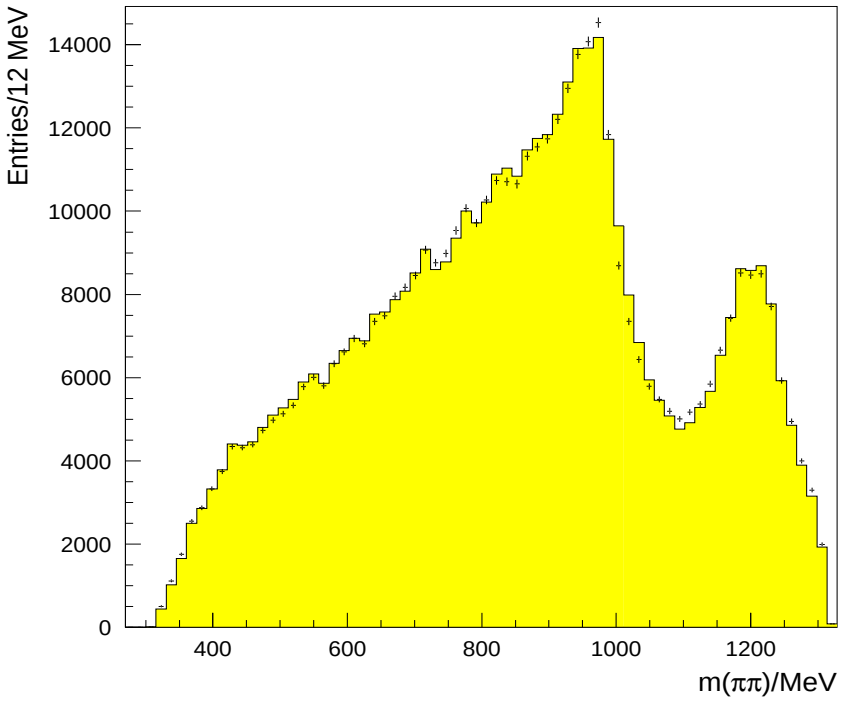

Figure 7: *Fit $\bar{p}p \to \pi^0\pi^0\eta$ in projection onto the $(\pi\pi)$-system for gaseous hydrogen data*

From 2-body-branching ratios and cascade model calculations [3, 4, 8], the changes of annihilation rates for every allowed protonium initial state depending on the target pressure are known. From multiple fits with random choice within errors of these ratios (see table 1) one obtains masses and widths of contributing resonances as given in table 2. Masses and widths of the $f_0(980)$ and $a_0(980)$ are derived from the speed plot, the phase difference per mass interval as a function of the mass, see figure 8 and figure 9.

	$f_0(980)$	$f_0(1370)$	$a_0(980)$	$a_0(1450)$	$a_2(1320)$	$a_2(1650)$	$\hat{\rho}(1390)$
M	996 ± 2	1240 ± 40	990 ± 8	1490 ± 15	1312 ± 8	1640 ± 20	1385 ± 15
Γ	100 ± 5	300 ± 50	80 ± 4	215 ± 35	105 ± 10	280 ± 30	150^{+100}_{-50}

Table 2: *Mass (M) and Width (Γ) of contributing resonances*

The analytical determination of the resonance parameters from complex energy planes of the Riemannian sheet for $f_0(980)$ for instance yields $[(930^{+10}_{-7})-i(34 \pm 8)]_{\mathrm{II}}$ and $[(985^{+20}_{-10})-i(30 \pm 4)]_{\mathrm{III}}$. The mass of $a_2(1320)$ is known to much higher accuracy [7]. Fixing it to nominal values yields comparable fits. This influences the parameters of most other resonances not more than whithin limits. Only the two yet ambigious resonances $f_0(1370)$ and $a_2(1650)$ appear to move in their mass and width. $f_0(1370)$ is found at M=1375 ± 20 and Γ=275 ± 25 and $a_2(1650)$ is then found at M=1555 ± 15 and Γ=160 ± 20.

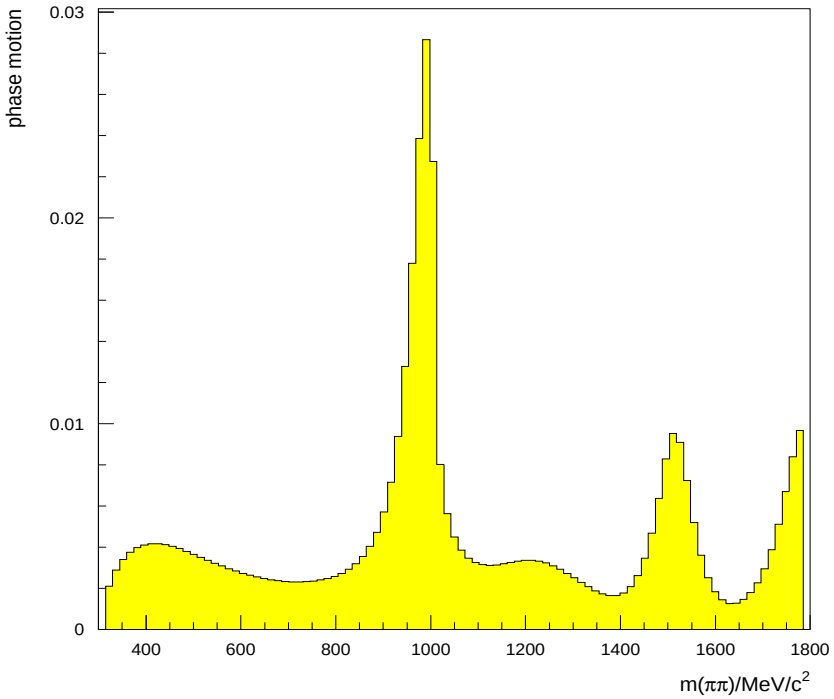

Figure 8: *Phase motion of scalar $(\pi\pi)$-wave*

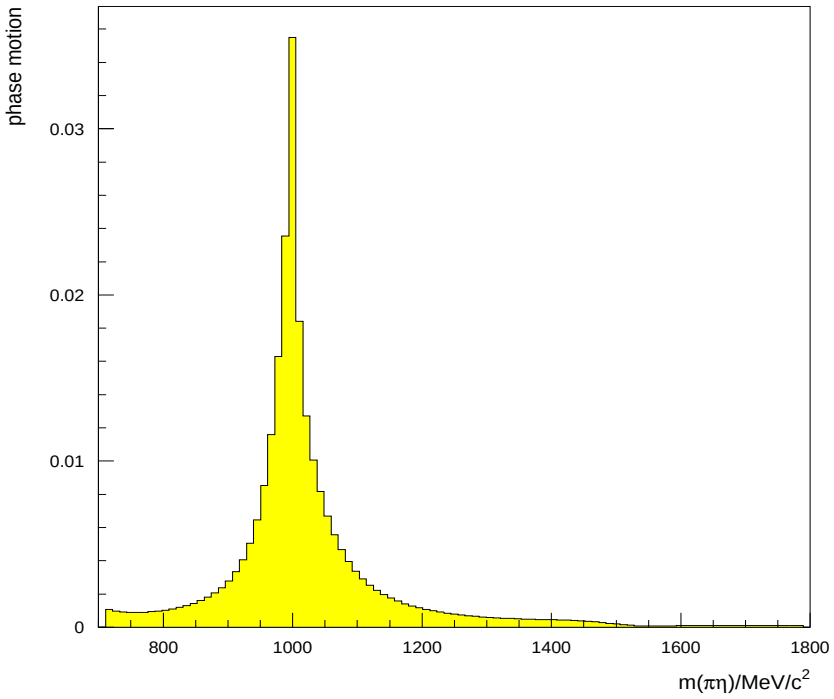

Figure 9: *Phase motion of scalar $(\pi\eta)$-wave*

The fractional contributions from all three possible initial states are given in table 3. We note that in this reaction, the P-state contribution is 10% when antiprotons are stopped in LH_2, underlining the dominance of S-state capture even though contributions from P-state are not negligible. The P-state contribution rises to 40% when going to GH_2 gas at 12 atm.

$^{2S+1}L_J$	LH_2	GH_2
$^1S_0$	$(89 \pm 5)\%$	$(59 \pm 5)\%$
$^3P_1$	$(5 \pm 2)\%$	$(21 \pm 3)\%$
$^3P_2$	$(6 \pm 2)\%$	$(19 \pm 3)\%$

Table 3: *intensity distribution of the $\pi^0\pi^0\eta$-final state according to the protonium cascade model*

The relative contribution of each resonance to the whole data set is given by the fraction of each individual amplitude squared over the sum of all amplitudes squared

$$R(i) = \frac{|A_i|^2}{\sum |A_j|^2} \tag{10}$$

Interferences of resonances contribute to the intensity distributions in our data as well. Therefore one is led to define the error for the above relative fraction in terms of

$$\frac{\Delta R(i)}{R(i)} = \left| \frac{|\sum A_j|^2 - \sum |A_j|^2}{\sum |A_j|^2} \right| \tag{11}$$

This way the partial wave analysis assigns the relative intensity fractions of the whole data sample to the resonances as listed in table 4. The second systematic error for the fraction attributed to $\hat{\rho}$ is derived from the systematic checks concerning the cascade model predictions for the coupling between the liquid hydrogen data and the gaseous hydrogen data and its width as described in the following subsection.

	LH_2	GH_2
$f_0(980/1370)\eta$	$(40.9 \pm 5.2)\%$	$(30.1 \pm 4.2)\%$
$f_2(1270)\eta$	$(1.0 \pm 0.1)\%$	$(4.0 \pm 0.6)\%$
$a_0(980)\pi^0$	$(13.6 \pm 1.7)\%$	$(10.0 \pm 1.4)\%$
$a_0(1450)\pi^0$	$(3.1 \pm 0.4)\%$	$(2.2 \pm 0.3)\%$
$a_2(1320)\pi^0$	$(37.5 \pm 4.8)\%$	$(47.9 \pm 6.7)\%$
$a_2(1650)\pi^0$	$(2.3 \pm 0.3)\%$	$(4.5 \pm 0.6)\%$
$\hat{\rho}(1390)\eta$	$(1.9 \pm 0.2^{+2.0}_{-1.0})\%$	$(4.9 \pm 0.7^{+3.0}_{-1.5})\%$

Table 4: *Intensity distribution to the $\pi^0\pi^0\eta$-final state*

Two remarks remain.

The intensity of $\hat{\rho}$ in gaseous hydrogen data is fitted to be larger than in liquid hydrogen data. However, the χ^2 variation allows to set the intensity to small values. Hence, the statistical significance stems from the transition $^1S_0 \to \pi\hat{\rho}$, not from P-state annihilation.

Even for a small amplitude of $\hat{\rho}$ the overall intensity from interferences with a large amplitude may very well be significant.

5.1 Evidence for the exotic state $\hat{\rho}$

The need for introducing the additional exotic $(\eta\pi)$-wave is discussed in the ongoing text. Beyond the two scalar resonances $a_0(980)$ and $a_0(1450)$ plus the two tensor resonances $a_2(1320)$ and $a_2(1650)$ no additional isovector 0^{++} or 2^{++} resonances are expected. Introducing further resonances with these quantum numbers do not improve the description of the data. However, there is need for additional intensity in the $(\eta\pi)$-subsystems. It is this need which drives the introduction of the exotic $(\eta\pi)_P$-wave, the evidence for which will be discussed below.

Figure 10 shows the simulated angular distribution for the a_2-resonance produced from initial $^1S_0$-state. The characteristic w-shapes of both $(\eta\pi)$-subsystems interfere constructively at high $(\eta\pi)$-invariant masses. The maximum of this distribution is not located at

the a_2-mass itself but is reduced due to overlapping tails of both nearby a_2-waves. The experimental data shown in figure 11 have a different shape. So there is a strong forward-backward asymmetry in the $a_2 \to \eta\pi$ decay. However, most of this asymmetry can be explained conventionally. For high $(\eta\pi)$-invariant masses there is destructive interference betweeen the a_2 and the low mass part of the scalar wave of $(\pi\pi)$-interaction, the only partial wave present in this kinematic region. For low $(\eta\pi)$-invariant masses there could be constructive interference with $f_0(1370)$ and $f_2(1270)$. The Dalitz plot cannot be fully described by only using known resonances. An additional amplitude is needed.

Figure 12 shows the differences of intensities between data and fit results when $\hat{\rho}(1390)$ is not included. There is missing theoretical intensity in the $(\eta\pi)$-subsytem for an invariant mass squared of about 1.9 $(\mathrm{GeV/c^2})^2$ overlapping constructively on the main diagonal of the Dalitz. For comparison reasons we show in figure 13 the intensity assigned to $\hat{\rho}(1390)$ when it is included in the fit. Both patterns are very similar. This shows that the poorly described experimental intensity without the $\hat{\rho}$ is distributed over the Dalitz plot in the same way as the expected contribution of the $\hat{\rho}$. By omitting the $\hat{\rho}(1390)$ from the fit the χ^2 deteriorates by 828 for LH_2 data and 128 for GH_2 data. This is highly significant. The need for introducing $\hat{\rho}(1390)$ can also be seen directly from invariant mass plots. Figure 14 shows the $(\eta\pi)$ invariant mass squared when the $(\eta\pi)$ invariant mass is (1390 ± 50) $\mathrm{MeV/c^2}$ compared to the fit without the $\hat{\rho}$. The missing intensities are filled up when feeding in the additional exotic wave. The χ^2 decreases and we find no more systematic deviations between data and fit, see figure 15. Then the $\hat{\rho}$ mass converges at 1390 $\mathrm{MeV/c^2}$ with a width of 150 $\mathrm{MeV/c^2}$.

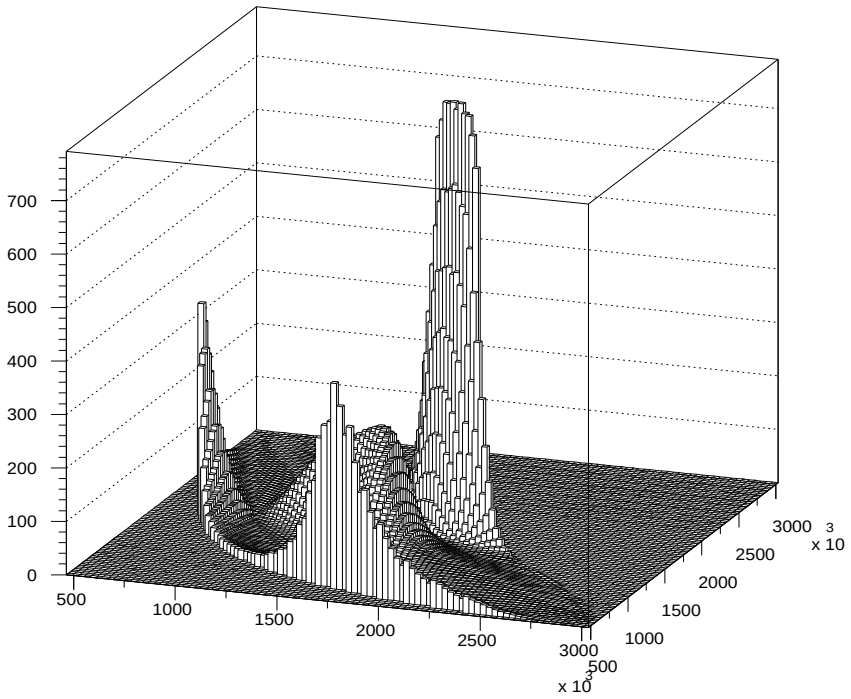

Figure 10: *Generated* $a_2(1320)$ *angular distribution from initial S-state*

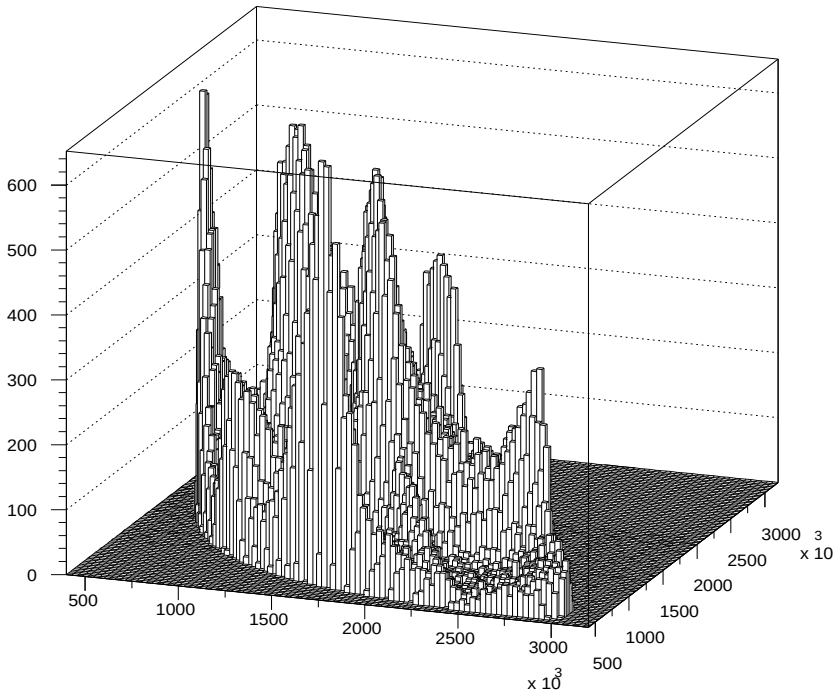

Figure 11: $\pi^0\pi^0\eta$ *experimental data*

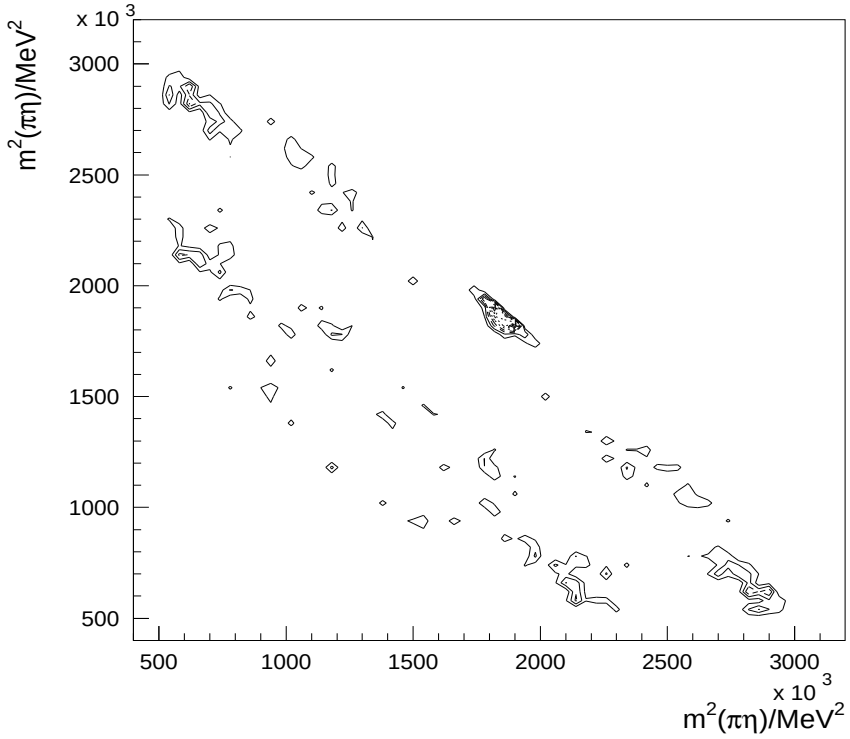

Figure 12: *Locations of insufficient description of data when omitting* $(\eta\pi)_P$*-wave in the fit*

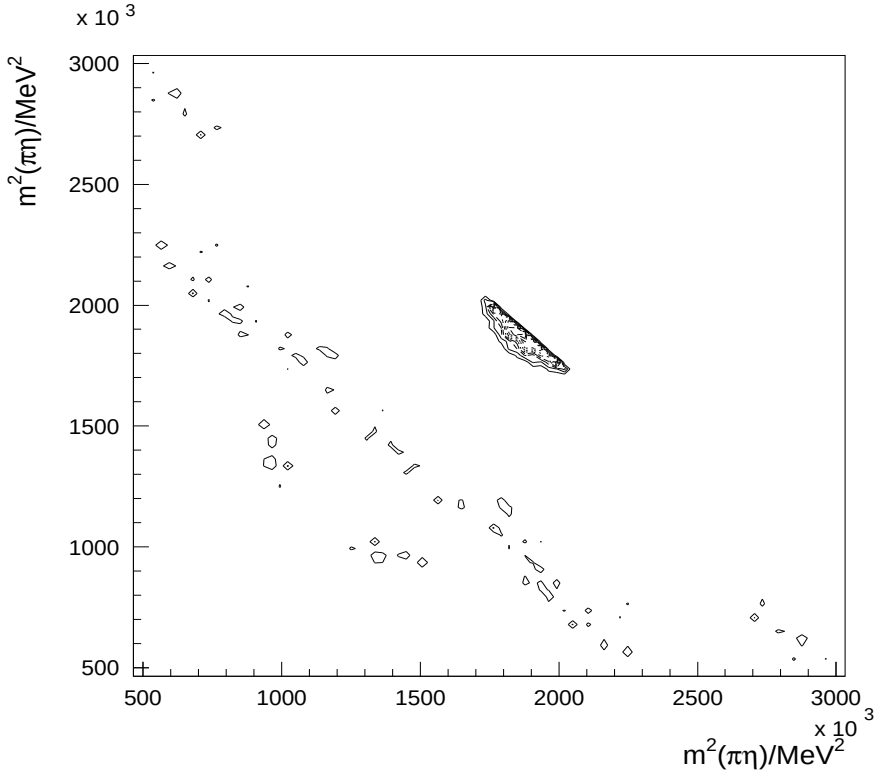

Figure 13: *Contribution of* $(\eta\pi)_P$*-wave in the fit*

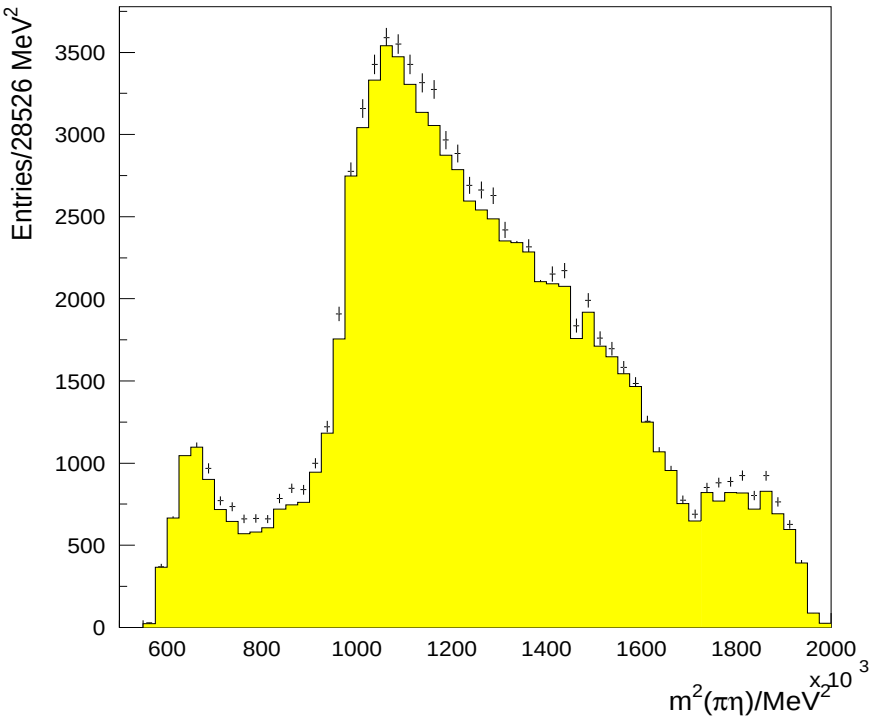

Figure 14: *Data and fit in a mass intervall of* (1390 ± 50) *MeV/c*^{2} *omitting* $\hat{\rho}(1390)$

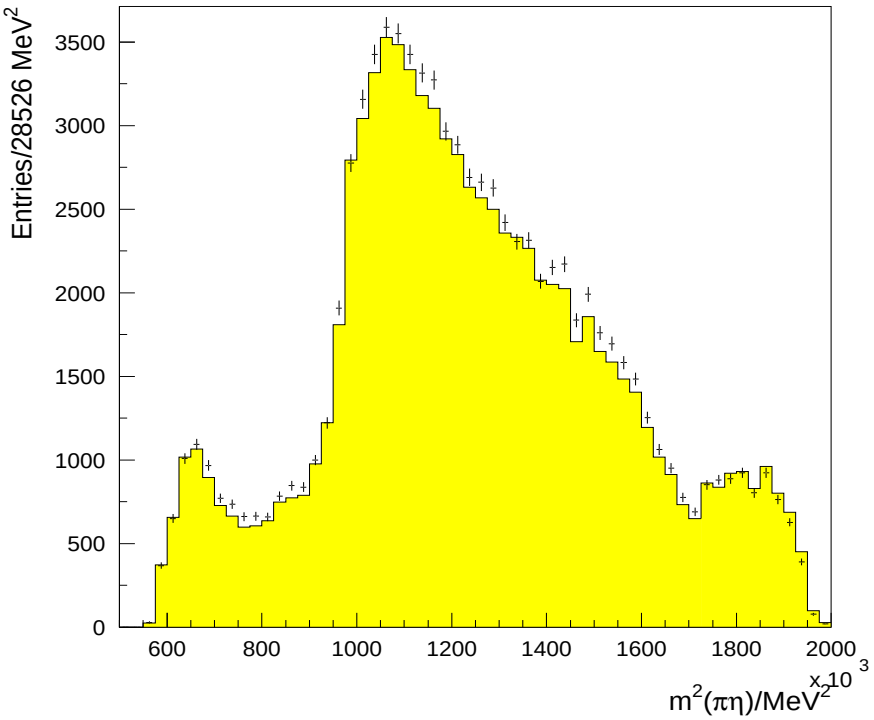

Figure 15: *Data and fit in a mass intervall of* (1390 ± 50) *MeV/c*^{2} *including* $\hat{\rho}(1390)$

Figure 16 shows the increase in χ^2 as a function of the $\hat{\rho}$ width. The entry for zero width corresponds to no $\hat{\rho}$ in the fit. The sharp minimum near 150 MeV/c^2 is dependent upon the cascade model input for the relative strengths of the initial atomic states in both LH_2 and GH_2. These values have been varied by $\pm 15\%$ and the above fits repeated. All require the presence of the $\hat{\rho}$. From this variation, the width can fall between 100 MeV/c^2 and 250 MeV/c^2 with an upper limit of 400 MeV/c^2. These values are consistent with a mass of 1400 MeV/c^2 and a width of 310 ± 50 MeV/c^2 as observed by us in deuterium.

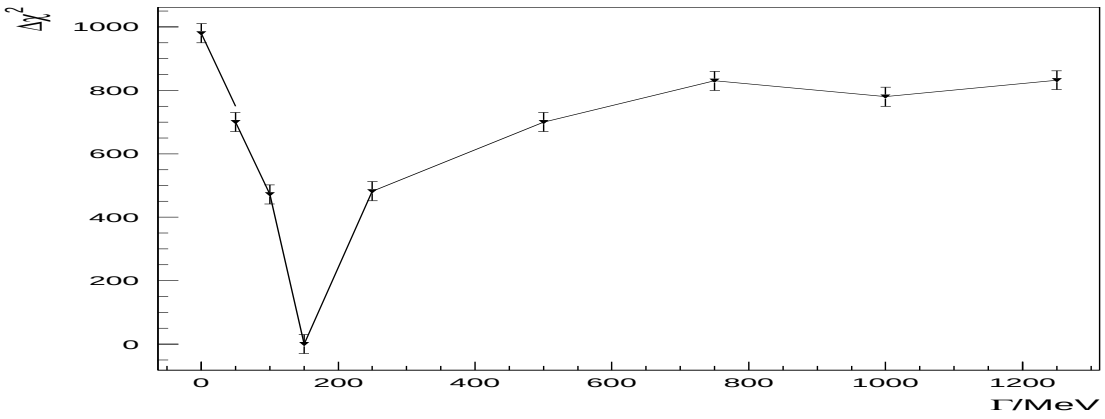

Figure 16: *χ^2-dependence of the hadronic width of $\hat{\rho}$(1390)*

References

[1] G. Reifenröther, E. Klempt
Nucl. Phys. A503, 885, **1989**

[2] J.M. Richard and M.E. Sainio,
Phys. Lett. B110, 349, **1982**

[3] C.J. Batty,
Nucl. Phys. A601, 425, **1996**

[4] U. Gastaldi and M. Placentino,
Spontaneous Polarization in $\bar{p}p$ Annihilations at Rest in H_2 Targets,
appearing in Nucl. Phys. A **1997**

[5] S.U. Chung et al.,
Partial Wave Analysis in K-matrix formalism,
Ann. Phys. 4, 404, **1995**

[6] G. Grayer et al.,
Nucl. Phys. B75, 189, **1974**

[7] Particle Data Group,
Phys. Rev. D54, **1996**

[8] M. Herz,
Evidenz fuer ein exotisches Meson mit den Quantenzahlen J^{PC}=1^{-+} in der Protonium-Vernichtung in Ruhe,
Universität Bonn, Dissertation, **1997**